J Mater Sci: Mater Electron (2012) 23:681–687
DOI 10.1007/s10854-011-0471-1

Effect of TiO_2 nanoparticles on the microstructure and bonding strengths of Sn0.7Cu composite solder BGA packages with immersion Sn surface finish

L. C. Tsao · M. W. Wu · S. Y. Chang

Received: 30 April 2011 / Accepted: 15 July 2011 / Published online: 24 July 2011

Abstract This study investigated the effects of TiO_2 nanoparticles on the interfacial microstructures and bonding strength of Sn0.7Cu (SC) composite solder joints in ball grid array packages with immersion Sn surface finishes. The addition of TiO_2 nanoparticles to SC solders resulted in significant changes in the interfacial microstructure. The nanoparticle addition suppressed the growth of the Cu_6Sn_5 IMC layer, significantly improving shear strength and reliability of solder joints after multiple reflows. The fracture surfaces of the SC solder exhibited a semi-brittle fracture mode with a relatively smooth surface, while those of the SC composite solder showed typical ductile failures with very refined dimpled surfaces.

1 Introduction

Ball grid array (BGA) solder interconnections are currently important in the microelectronics industry. In some BGA packages, solder balls are used to form solder bumps on top of the under bump metallization (UBM) of the BGA. The solder bumps are then soldered onto the metal pads of a substrate such as a printed circuit board (PCB) for electrical connection. Among the many Pb-free solder alloys, the eutectic Sn–Cu solder (Sn0.7Cu wt%) is considered the most promising candidate alloy to replace the eutectic Sn–Pb solder for wave soldering [1, 2]. This solder is less expensive than Sn–Ag and Sn–Ag–Cu solders, but the melting temperature is slightly higher [3].

Recently, lead-free solders doped with nano-sized, nonreacting, noncoarsening oxide dispersoids have been identified as potential materials to provide higher microstructure stability and better mechanical properties as compared to conventional solders [4–20]. Zhong and Gupta [4] demonstrated that the mechanical properties (microhardness, 0.2% YS, and UTS) increase with the increasing presence of reinforcement, with the best tensile strength, realized in the composite containing 1.5% alumina, far exceeding the strength of the eutectic Sn–Pb solder. Tsao et al. [5–7] reported that the addition of TiO_2 and Al_2O_3 nanopowders into a Sn–Ag–Cu solder reduced the average size and spacing of Ag_3Sn particles significantly. Shen et al. [8] investigated the Sn–3.5Ag–ZrO_2 composite solders and found that the size of dendrite β-Sn grains and intermetallic compounds (IMC) was refined.

Actually, the metallurgical reaction between liquid solder and copper, or other metallization, results in an IMC layer at the joint interface. Although the formation of a thin IMC layer is desirable to achieve good metallurgical bonding, it is known that thicker IMC growth affects the mechanical reliability in ball grid array (BGA) and flip-chip solder joints. This problem of IMC overgrowth has a deleterious effect in the case of Pb-free solders [8–11]. However, when a small amount of La (only 0.05 wt%) is added into Sn40Pb solder alloy, the growth of Cu–Sn IMC at the solder joint interface is depressed, and the thermal fatigue life of solder joints is improved [10]. Chuang et al.

L. C. Tsao (✉)
Department of Materials Engineering, National Pingtung University of Science and Technology, 1, Hseuhfu Road, 91201 Neipu, Pingtung, Taiwan
e-mail: tlclung@mail.npust.edu.tw

M. W. Wu
Department of Materials Science and Engineering, National Formosa University, Huwei, Yunlin 632, Taiwan

S. Y. Chang
Department of Mechanical Engineering, National Yunlin University of Science and Technology, 64002 Touliu, Yunlin, Taiwan

reported that the interfacial IMC layers in Sn58Bi0.5La solder joints were much thinner than those in undoped Sn58Bi [12]. In addition, our findings correspond to similar results presented by Nai et al. [13], who studied the suppression of IMC growth by the addition of carbon nanotubes (CNTs).

In this study, a small amount of TiO_2 nanoparticles was added to the Sn0.7Cu (SC) based solder to produce a new solder alloy. The interfacial intermetallic reactions, bonding strengths, and fracture mode of SC composite solder ball grid array (BGA) solder joints after different reflowing processes were investigated.

2 Experimental

The BGA package used in this study had 49 Cu pads on a FR-4 substrate, and the surfaces of the Cu pads were immersion-plated with 0.2 µm thick Sn film. The solder mask-opening diameter was 550 µm. The SC composite solders were prepared via mechanically dispersing 0.5 and 1.0 wt.% of TiO_2 nanoparticles of about 20 nm in diameter (Nanostructured & Amorphous materials, USA) into SC solder paste. The intermixtures were blended manually for at least 45 min to uniformly distribute the TiO_2 nanoparticles with a water-soluble flux (Qualitek Singapore (PTE) Ltd.). Then the paste intermixture was printed onto alumina substrates using a 150 µm-thick stainless steel solder paste stencil and reflowed in a reflow oven (Reddish Electronic, SM2000CXE) at 250 °C to prepare solder balls of about 0.76 mm in diameter. SC composite solder (wt%) solder balls were dipped in rosin mildly activated (RMA)-type flux, placed on these Sn/Cu pads, and then reflowed in a hot-air furnace (Reddish Electronic, SM2000CXE).

The reflow temperature profile, with a peak temperature at 267 °C for a melting time of 90 s ($T_m > 229.7$ °C), is shown in Fig. 1. All samples were divided into two groups: one cycle and eight cycles of reflow.

All samples were cross-sectioned through a row of solder balls, ground with 2,000-grit SiC paper, polished with 1 and 0.3 µm Al_2O_3 powders, and etched with 5% HCl and 95% H_2O solution. The morphology of the intermetallic compounds was observed by scanning electron microscopy (SEM). The mean thickness of the interfacial IMC was evaluated using image analysis software.

The bonding strengths of the solder joints in the BGA packages after reflowing were tested using Dage 4000 pull test machine, for which the shear rate and shear height were set at 0.1 mm/s and 125 µm (about 1/4 of the reflowed ball height), respectively. Figure 2 shows a schematic illustration of the ball shear test performed in this study. The fractography of the solder joints after ball shear testing was observed by SEM.

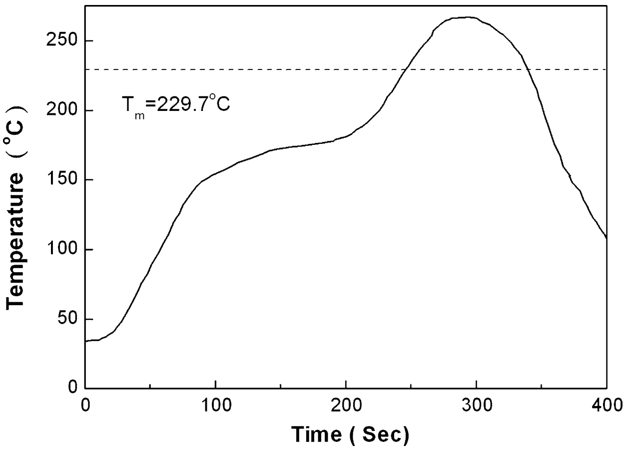

Fig. 1 Temperature profile for reflowing the SC composite BGA packages in this study

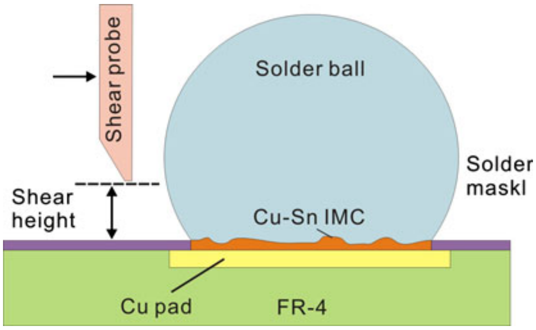

Fig. 2 Schematic illustrations of the ball shear test

3 Results and discussion

The microstructures of the SC composite solder balls before reflow are shown in Fig. 3. The microstructure of SC solder balls consists of β-Sn phases, needle-like Cu_6Sn_5 IMCs, and eutectic areas. As shown in Fig. 3b and c, the SC composite solder balls had a finer microstructure than that of SC solder balls. Notably, the sizes of the Cu_6Sn_5 IMCs decreased with increases in the amount of TiO_2 nanoparticles. As is well known, a notable effect of nanosized, nonreactive, noncourse nanoparticles on solder alloys is to refine the microstructure [14, 15]. The theory of heterogeneous nucleation can also be used to explain the refinement of Cu_6Sn_5 particles in the prepared SC composite solder. Hao et al. [16] reported that $ErSn_3$ IMCs formed from the molten solder provided heterogeneous nucleation sites for the IMCs in the soldering. Subsequently, the Cu–Sn IMCs produced during soldering have a uniform size and are evenly distributed in the solder matrix. A similar result was also reported by Wang et al. [17]. This phenomenon indicates that the TiO_2 nanoparticles could improve the microstructure and the reliability of the SC composite solder joints in service [18].

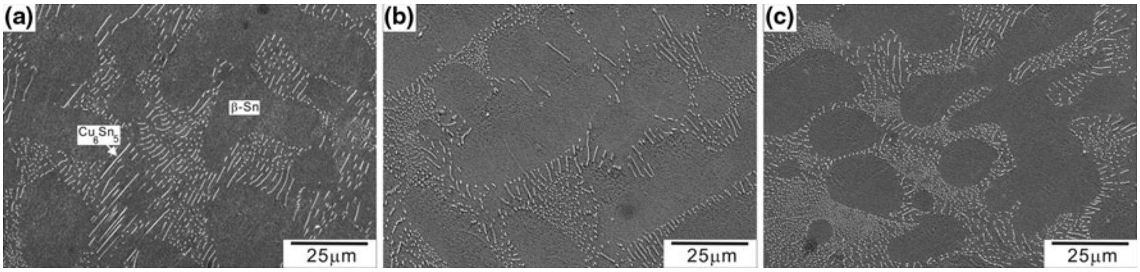

Fig. 3 SEM micrographs of SC composite solders: **a** SC, **b** SC-0.5TiO_2, and SC-1TiO_2

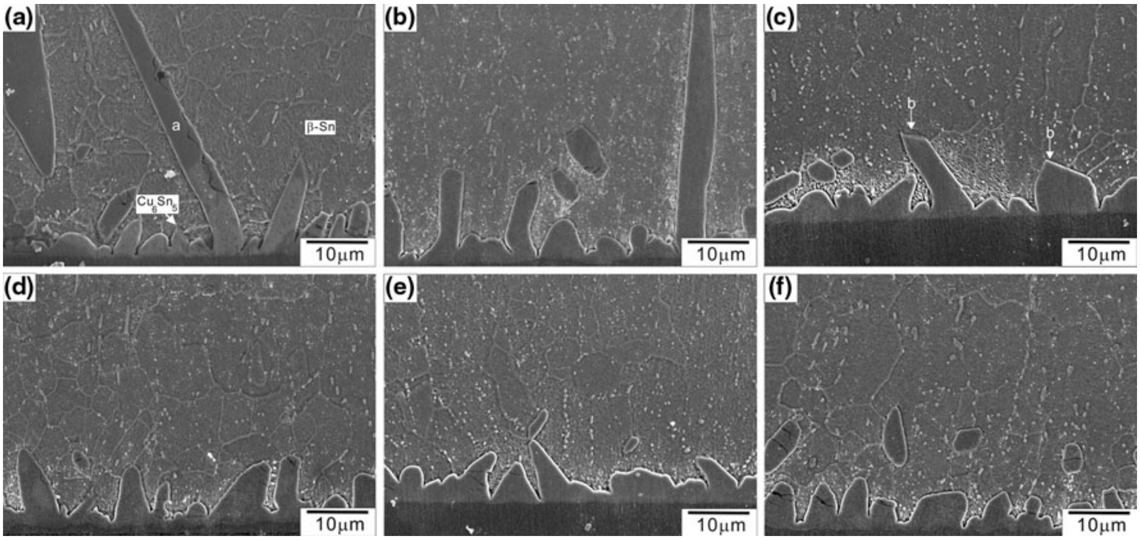

Fig. 4 Interfacial microstructures of the SC composite solder joints after one (**a**, **c**, **e**) and eight (**b**, **d**, **f**) cycles of reflowing: **a**, **b** SC, **c**, **d** SC-0.5TiO_2, **e**, **f** SC-1TiO_2

Cross-sectional microstructures of the three types of solder joints are shown in Fig. 4, in which one cycle and eight cycles of reflow are compared. After reflowing, the immersion Sn thin film on the Sn/Cu pads has dissolved into the solder matrix, and a Cu_6Sn_5 IMC layer has formed at the SC composite solder/Cu interface. It can be seen in Fig. 4a that the Cu_6Sn_5 IMC layer has grown into an elongated shape, and wicker-Cu_6Sn_5 IMCs (mark a) have grown into the solder matrix. The wicker-Cu_6Sn_5 IMCs in these images were several hundreds of micrometers in length. Kim et al. [8] reported that large Ag_3Sn and long Cu_6Sn_5-whiskers are formed in all SAC/Cu joints and in high Cu-content solder joints. These large or long IMCs induce brittle fracturing at an interface and provide crack initiation sites. However, how the complex growth mechanisms govern the formation and morphological evolution of the interfacial layers is still unclear [19–21]. These authors had reported that wicker-Cu_6Sn_5 IMCs were also observed in solidified tin and noted to emanate from the tops of the Cu_6Sn_5 scallops. It is suggested that the formation of the wicker-Cu_6Sn_5 IMCs emerging from the scallop tops is related to a local concentration increase in copper, and that they grow into the solder matrix by the reaction of tin (Sn) with this copper (Cu). Nucleation is not required because they grow from the tops of the scallops, and in the same crystal orientation as the scallops. This could be attributed to the following [20–22]: (1) The soldering process provides access for diffusion of Cu and Sn atoms and thus causes solidification from preferred growth, with the crystallographic c-axis pointing along the concentration gradient; and (2) the formation of wicker-Cu_6Sn_5 IMCs could be due to a reduction of the copper concentration in the liquid. However, wicker-Cu_6Sn_5 IMCs would be adverse to the reliability of the solder joints.

The addition of a small percentage of TiO_2 nanoparticles alters the lead-free SC composite solder/pad interface morphology after one time of reflow, as shown in the SEM micrographs in Fig. 4c and e. It is clear that the long wicker-Cu_6Sn_5 IMCs disappeared at the interface with an increase in the content of TiO_2 nanoparticles to 0.5–1 wt%. After eight cycles of reflow, the morphology of the Cu_6Sn_5 IMC layer changed from regular prism-type (mark b) to scallop-type (Fig. 4d, f). Suh et al. [23] studied the size distribution and morphology of Cu_6Sn_5 IMC layers in wetting reactions between molten solder and copper. The morphology of the Cu_6Sn_5 IMCs was dependent on the composition of the solder. When the Pb content was further decreased <30 wt%, faceted scallops were observed along with some round scallops. Finally, when the solder became pure tin, only faceted scallops were observed. Wang et al. [24] reported that the growth of scallop-type grains is mainly caused by the ripening flux, while the growth of prism-type grains is caused by the interfacial reaction flux. Bian et al. [25] have found that there exists not only short-range order (SRO) but also medium-range order (MRO) in liquid metals. Also, Zhao et al. [26] found no MRO and a liquid structure in molten Sn0.7Cu solder similar to that of pure Sn, while for Sn_2Cu solder, the MRO Cu_6Sn_5 clusters at 260 °C have a great contribution to the liquid structure. The MRO in liquid solder quickens the formation of interfacial IMCs in the very early stage of soldering and also accelerates the ripening process of IMC grains at the interface. In our experiment, the Cu concentration of SC composite solder is similar to pure Sn under one cycle of reflow, so there may also have been SRO Cu_6Sn_5 in the SC composite solder. However, the Cu concentration in the SC composite solder ball matrix increased under eight cycles of reflow. There may have been both SRO Cu_6Sn_5 clusters and MRO Cu_6Sn_5 clusters in the liquid solder. Thus, since the Cu concentration of the SC composite solder ball matrix was enhanced, there may have been, in addition to SRO Cu_6Sn_5 clusters, MRO Cu_6Sn_5 clusters in the liquid solder. This indicates that the MRO Cu_6Sn_5 in liquid solder quickens formation of the scallop Cu_6Sn_5 grains in the ripening process at the interface. As a result, the morphology of the IMC layer formed in the SC composite solder/Cu joints changed from prism-type to scallop-type after multiple cycles of reflowing.

The thicknesses of the Cu_6Sn_5 IMC layers at the solder/pad interfaces of the SC composite solder packages versus added wt% of TiO_2 nanoparticles are also summarized in Table 1 and shown in Fig. 5. The average thickness of the IMC layer was calculated using the following equation: $T = S/L$, where L is the length measured, and S is the integral contour area of the IMC layer at the interface. With multiple reflows, the thickness of the IMC layer increased with increasing number of reflow cycles. In addition, it was observed that the IMC layer thickness of SC composite solder joints decreased with an increase in the addition of TiO_2 nanoparticles into a SC solder mixture. Nai et al. [27–32] studied the suppression of CNTs on the growth of IMC layers between Sn3.5Ag0.7Cu composite solders and Cu pads after aging. Liu et al. [29] reported that the dispersion of Y_2O_3 degrades the grain boundary migration activation energy, and the size of the Cu_6Sn_5 particles and the thickness of Cu_6Sn_5 IMC layer decrease. Shen and Chen [30] added nano-sized ZrO_2 particles into a Sn9Zn solder to suppress the growth of Ni–Zn IMC in Sn9Zn/Ni solder joints. This suggests that the TiO_2 nanoparticles suppressed the growth of the Cu_6Sn_5 IMC layer.

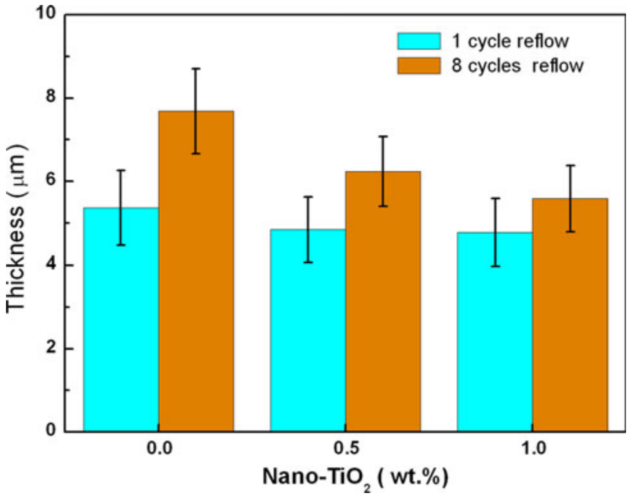

Fig. 5 IMC layer thickness of SC composite solder joints

Table 1 The overall thickness of Cu–Sn IMC layer of the Sn0.7Cu composite solder BGA packages with Ag/Cu after different numbers of reflow cycles

Sample #	Addition (wt%)	Cu–Sn IMC layer (μm)	
		Reflow 1	Reflow 8
SC	Nil	5.37 ± 0.89	7.69 ± 1.02
1	0.5	4.85 ± 0.78	6.24 ± 0.84
2	1	4.78 ± 0.81	5.59 ± 0.79

The average shearing forces of the SC composite solder joints are summarized in Table 2 and plotted in Fig. 6. The average shear strength of the SC composite solder joints after eight cycles of reflow was higher than that of the SC composite solder joints after 1 cycle of reflow by about 2.6% in SC solder, 9.4% in SC-0.5TiO_2 solder, and 10.8% in SC-1TiO_2 solder. In addition, the changes in shearing forces with larger additions of TiO_2 nanoparticles into the solder matrix are clear. When the TiO_2 nanoparticle content is at 1 wt%, after one cycle and eight cycles of reflow,

Table 2 Ball Shear strength of the Sn3.5Ag0.5Cu composite solders

Sample #	Addition (Wt%)	Ball Shear strength (N)	
		Reflow 1	Reflow 8
SC	Nil	8.15 ± 1.21	8.76 ± 1.34
1	0.5	8.55 ± 0.96	9.35 ± 1.26
2	1	8.8 ± 1.12	9.75 ± 0.98

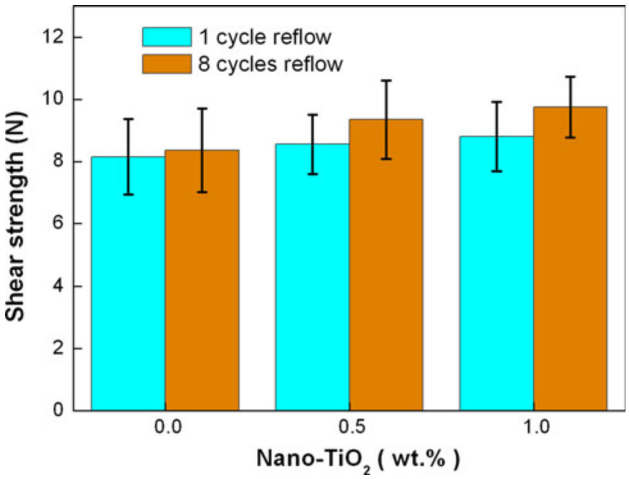

Fig. 6 Variation of average shear strengths of SC composite solder joints

shear strengths show increases of 8.0 and 11.3%, respectively. It is suggested that repeated reflow cycles enhance the larger shearing area due to enlargement of the contact area and reduction in the height of the solder joints. Thus, the shear strength is raised. Moreover, multiple cycles of reflowing may enhance Cu interdiffusion, allowing it to react rapidly with Sn and precipitate Cu_6Sn_5 IMC in the solder ball matrix. Another important point is that addition of TiO_2 nanoparticles could promote a high nucleation density of stable second-phase dispersoid particles (TiO_2 and Cu_6Sn_5) in solder ball joins. As a result, both TiO_2 nanoparticles and Cu_6Sn_5 IMC act as potential sites that (1) pin grain boundaries, thereby impeding sliding of the grain boundaries, and (2) increase the number of dislocation densities and obstacles, thereby restricting the motion of dislocation [5, 31]. It should also be noted that the shear strength increased in the SC composite solder joints. Zhong, et al. [32] has reported that the shearing forces of the Sn37Pb and Sn3Ag0.5Cu solder joints tend to increase slightly with an increase in the number of reflow cycles due to diffusion-induced solid solution strengthening of the bulk solder and augmentation of the shearing area.

Figures 7 and 8 show typical fractography of the SC composite solder joints in BGA packages after 1 and 8 cycles of reflow, respectively. Figure 7a and b shows the typical semi-brittle fracture mode with a relatively smooth surface (mark A), coarse IMC (mark B), and very rough dimples (mark C) occurring in the SC solder after one cycle of reflow. In addition, the Cu_6Sn_5 IMC particles can be seen clearly at the center of each dimple. It can be speculated that the crack initiates and propagates at the brittle Cu_6Sn_5 IMC in an early stage of the shearing. As a result, the typical fracture is seen as a combination of solder shear and solder/Cu_6Sn_5 IMC separation (mark D). Hence, the average shearing force is lower than only that of SC composite solder joints [33].

However, after the addition of TiO_2 nanoparticles, the fracture mode of the SC composite solder was dramatically changed. When 0.5 wt% TiO_2 nanoparticles was added, the fracture mode clearly appeared to have a rough surface, small dimples, and a small partial ductility fracture in the edge area of the joint; i.e., the ductile fractured dimples throughout the matrix, as shown in Fig. 7c and d. From Fig. 7e and f, it is confirmed that the fracture surface of the SC-1TiO_2 composite solder joints exhibited a larger ductility fracture with a smaller dimple surface. The fracture occurred in all the solder joints as cracks propagated through the SC composite solder balls, which ruptured

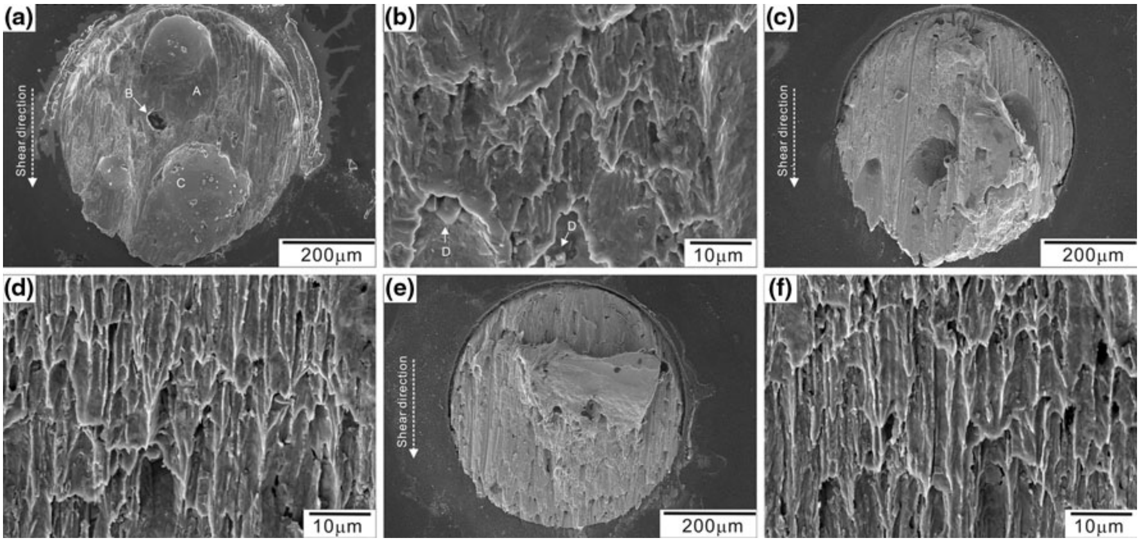

Fig. 7 Typical fracture surfaces of the SC composite solder joints after one reflow cycle: **a**, **b** SC, **c**, **d** SC-0.5TiO_2, and **e**, **f** SC-1TiO_2

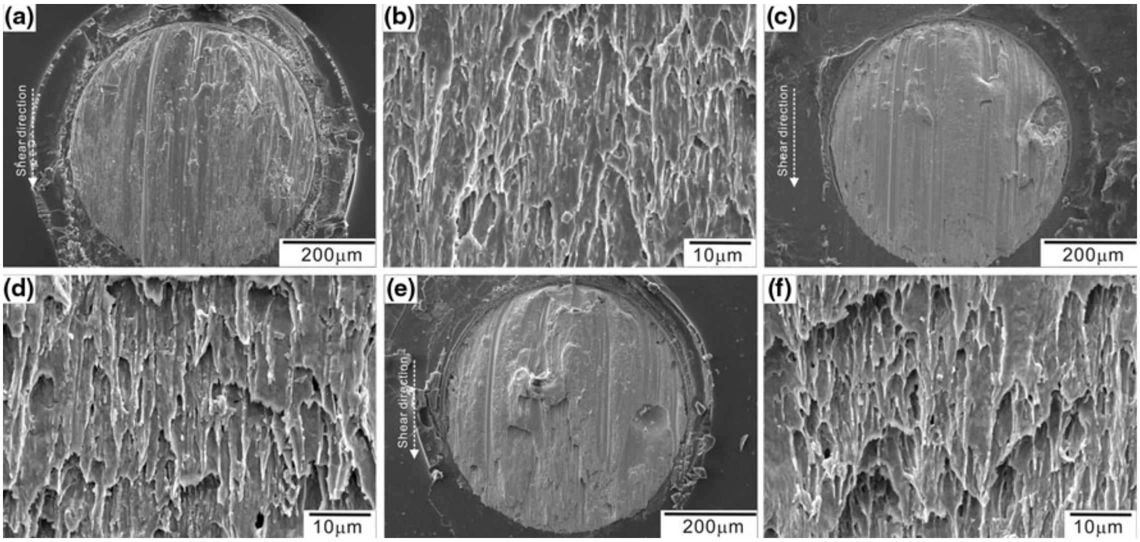

Fig. 8 Typical fracture surfaces of the SC composite solder joints after eight reflow cycles: **a**, **b** SC, **c**, **d** SC-0.5TiO_2, and **e**, **f** SC-1TiO_2

mostly along the submicro Cu_6Sn_5 IMCs and solder matrix. This indicates that the solder/pad bond is much stronger than the shear strength of the bulk solders.

On the other hand, the fracture mode of the SC composite solder joints changed obviously after eight cycles of reflow, as shown in Fig. 8. The fracture surfaces of SC solder joints after eight cycles of reflow exhibited a brittle fracture with a smooth surface, as shown in Fig. 8a and b. However, with the addition of TiO_2 nanoparticles, the fracture mode exhibited a typical ductile characteristic and a finer dimple surface, as shown in Fig. 8c and f. The schematic diagrams shown in Fig. 9 summarize the two fracture modes: A fracture surfaces of the solder joints revealed that the crack propagation occurred above the IMC/solder interface and revealed the dimple formation mechanism. Crack propagation along the intermetallic interface in the SC composite solders does not take place. This is likely a result of stresses within the solder being more homogeneously distributed and not concentrated at the IMC/solder interface. Thus, in SC composite solder, the fracture surfaces appeared to be ductile, with very fine dimpled surfaces, due to the homogeneous distribution of TiO_2 particles. Such enhanced ductility has profound implications for improving the mechanical shock resistance (such as drop failure) of electronic packages containing SC composite solders.

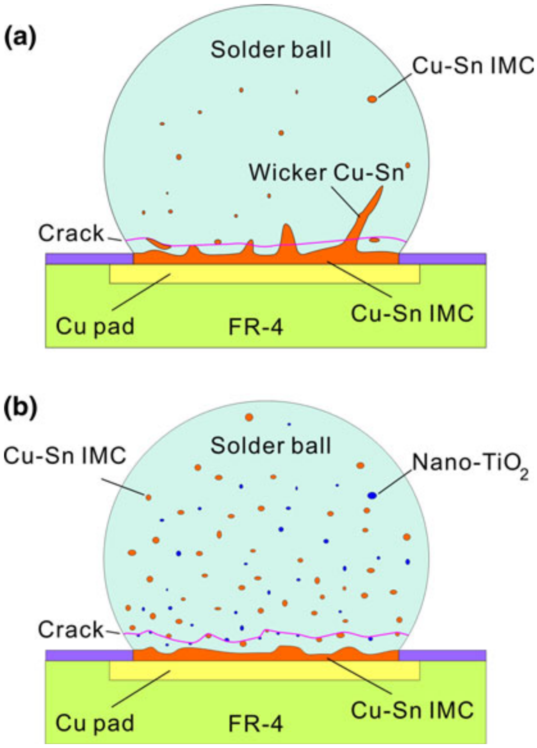

Fig. 9 Schematic drawing of shear fracture modes of BGA solder joints: **a** SC solder, **b** SC composite solder

4 Conclusions

In the present work, the interfacial reaction, morphology of IMCs, and shear strength of SC composite solder and BGA substrates with different numbers of reflow cycles were investigated. In addition, a more uniform microstructure of solder alloys has been obtained in SC composite solder. A continuous layer of elongated-shaped Cu_6Sn_5 IMCs was found at the interfaces in the SC solder joints after different numbers of reflow cycles, and wicker-Cu_6Sn_5 IMCs grew into the solder matrix. It was found, however, that the addition of small amounts of TiO_2 nanoparticles to SC solders changes the morphology of the IMC layer by eliminating the wicker-Cu_6Sn_5 IMCs and suppressing the growth of the Cu_6Sn_5 IMC layer. After multiple cycles of reflowing, the morphology of the IMC layer formed in SC composite solder/Cu joints changes from prism-type to scallop-type, and the average shear force is enhanced by about 2.6% in SC solder, 9.4% in SC-0.5TiO_2 solder, and 10.8% in SC-1TiO_2 solder. As a result, the shear strength of SC composite solder joints is improved. Despite the multiple reflow cycles, the fracture surface of SC solder exhibited a semi-brittle fracture mode with a relatively smooth surface, while SC composite solder showed typical ductile failures with very refined dimpled surfaces.

References

1. K. Zeng, K.N. Tu, Mater. Sci. Eng. R. **38**, 55–105 (2002)
2. W.T. Chen, C.E. Ho, C.R. Kao, J. Mater. Res. **17**, 263–266 (2000)
3. M. Abtew, G. Selvaduray, Mater. Sci. Eng. **27**, 95–141 (2000)
4. X.L. Zhong, M. Gupta, J. Phys. D: Appl. Phys. **41**, 095403–095409 (2008)
5. L.C. Tsao, S.Y. Chuang, Mater. Des. **31**, 990–993 (2010)
6. L.C. Tsao, S.Y. Chang, C.I. Lee, W.H. Sun, C.H. Huang, Mater. Des. **31**, 4831–4835 (2010)
7. T.H. Chuang, M.W. Wu, S.Y. Chang, S.F. Ping, L.C. Tsao, J. Mater. Sci: Mater. Electron. **22**, 1021–1027 (2011)
8. K.S. Kim, S.H. Huh, K. Suganuma, J. Alloys Compd. **352**, 226–236 (2003)
9. G. Ghosh, Acta Mater. **48**, 3719–3738 (2000)
10. X. Ma, Y.Y. Qian, F. Yoshida, J. Alloys Compd. **334**, 224–227 (2002)
11. W. Yang, L.E. Feltion, R.W. Messler, J. Electron. Mater. **24**, 1465–1472 (1995)
12. Y.Y. Shiue, T.H. Chuang, J. Alloys Compd. **491**, 610–617 (2010)
13. S.M.L. Nai, M. Gupta, J. Wei, in *Proceedings of the 2nd IEEE International Nanoelectronics Conference* (INEC), 2008, pp. 15–19
14. J. Shen, Y.C. Chan, Microelectron. Rel. **49**, 223–234 (2009)
15. H. Mavoori, S. Jin, J. Electron. Mater. **27**, 1205–1210 (1998)
16. H. Hao, Y. Shi, Z. Xia, Y. Lei, F. Guo, J. Electron. Mater. **37**, 2–8 (2008)
17. X. Wang, Y.C. Liu, C. Wei, H.X. Gao, P. Jiang, L.M. Yu, J. Alloys Compd. **480**, 662–665 (2009)
18. L.C. Tsao, J. Alloys Compd. **509**, 2326–2333 (2011)
19. T. Liu, D. Kim, D. Leung, M.A. Korhonen, C.Y. Li, Scripta Metall. **35**, 65–69 (1996)
20. M. Harada, R. Satoh, IEEE Trans. Comp. Hybrids Manuf. Tech. **13**, 736–742 (1990)
21. R.A. Gagliano, M.E. Fine, JOM **53**, 33–38 (2001)
22. A. Sharif, Y.C. Chan, J. Alloys Compd. **390**, 67–93 (2005)
23. J.O. Suh, K.N. Tu, G.V. Lutsenko, A.M. Gusak, Acta Mater. **56**, 1075–1083 (2008)
24. L. Wang, H. Xu, M. Yang, M. Li, Y. Fu, in *Proceedings of the 2009 International Conference on Electronic Packaging Technology & High Density Packaging (ICEPT-HDP)*, 2009, pp. 843–846
25. X.F. Bian, P.X. Min, X.B. Qin, M.H. Jiang, Sci. China **45**, 113–119 (2002)
26. N. Zhao, X.M. Pan, H.T. Ma, C. Dong, S.H. Guo, W. Lu, L. Wang, Phys.: Conf. Ser. **98**, 012029 (2008)
27. S.M.L. Nai, J. Wei, M. Gupta, J. Alloys Compd. **473**, 100–106 (2009)
28. S.M.L. Nai, J. Wei, M. Gupta, J. Electron. Mater. **35**, 1518–1522 (2006)
29. X.Y. Liu, M.L. Huang, C.M.L. Wu, L. Wan, J. Mater. Sci: Mater Electron. **21**, 1046–1054 (2010)
30. J. Shen, Y.C. Chan, J. Alloys Compd. **477**, 552–559 (2009)
31. H. Mavoori, S. Jin, Appl. Phys. Lett. **73**, 2290–2292 (1998)
32. W.H. Zhong, Y.C. Chan, B.Y. Wu, M.O. Alam, J.F. Guan, J. Mater Sci. **42**, 5239–5247 (2007)
33. L.C. Tsao, J. Alloys Compd. **509**, 8441–8448 (2011)